Supporting Information

Brinks et al. 10.1073/pnas.1308652110

SI Materials and Methods

The output of a broadband Ti:sapphire laser (Octavius 85M; Menlo Systems) was expanded and collimated with a set of spherical mirrors and fed into a double-pass 4f-pulse shaper based on an in-laboratory modified multiphoton intrapulse interference phase scan (MIIPS) box. A 120-nm spectral band centered around 776 nm of the laser output was dispersed with a grating and focused on a 640-pixel double-layer spatial light modulator (SLM). The light was reflected back through the SLM, recollimated and recombined, caught on an end mirror, and reflected back through the entire shaper. The shaper output was separated from the input with a polarizing beam splitter and directed through a Glan–Taylor polarizer to clean the amplitude modulation. The beam was subsequently spatially filtered using a telescope with a 100-μm pinhole.

The experiments were performed on a modified confocal microscope (Zeiss Axiovert). The shaped pulses were directed into the back port of the microscope and reflected into the sample with a short-pass dichroic mirror (SDi-01-670; Semrock). The pulses were focused into the sample plane with a 1.3 N.A. objective (Zeiss Fluar). The two-photon photoluminescence (TPPL) of the antennas was collected through the same objective, separated from the excitation light by the dichroic mirror and two short-pass filters (FF01-720SP-25 and FF01-660SP-25; Semrock) and focused on two polarization-split avalanche photodiodes (SPCM-AQRH-16; Perkin-Elmer).

Pulse calibration was done via the MIIPS method with a micrometer sized beta barium borate (BBO)-crystal plate in the sample plane. The second harmonic (SH) signal of the crystal plate was collected in transmission by an optical fiber and focused onto an imaging spectrograph with a sensitive CCD camera (SR-163 with camera DV437-BV; Andor). The calibration resulted in a compression mask: a phase added in the shaper to ensure a Fourier limited starting pulse in the sample plane; the pulse shapes used in the experiment were added on top of this. For calibration and measurement integration times of at least 20 s were used to ensure phase stability of the SH and TPPL signals.

The experiments were performed on gold nanoantennas of variable length, 50-nm width and 20-nm thickness. The sample was fabricated on 10-nm indium tin oxide on glass by e-beam lithography, thermal gold evaporation, and lift-off, according to a previously described procedure (1). On the same sample, matrices with repetitions of single antennas with varying lengths and coupled antennas with different ratios between bar lengths were alternated.

The sample was excited with an 85-MHz train of pulses centered at 776 nm with the spectral amplitude and phase as shown in Fig. 1*A*. The time-averaged power in the sample plane after spatial filtering and application of additional neutral density filters was 3.3×10^{-6} W, corresponding to a flux of ~2.8 kW/cm^2.

The antennas were excited with linear polarization along the antenna axis; in combination with the linear antennas this served to avoid any polarization effects.

At the start of each experiment the sample was scanned through the focus of the microscope objective with a piezo scanner (Nanoview/M 100-3; Mad City Labs), yielding TPPL images of the matrices of antennas with each hotspot lighting up. The experiments were performed by positioning one of the hotspots in the focus with the piezo scanner. Subsequently the phase shape of the pulse was changed, and the corresponding TPPL response of the antenna was recorded. Typically, all phase shapes were cycled with a 1-s integration time each. The measurement for every phase shape was alternated with an equally long measurement with a Fourier limited reference pulse. This ensures long total integration times for each signal point, and at the same time provides the time resolution and reference signal to monitor signal changes unrelated to the experiment. Depending on the antenna and its resonance, the signal was between 2.5 and 6.5 kcts/s. For the data from Figs. 2 and 3, this cycle was repeated between 20 and 30 times; each cycle consisted of 64 measurements of different phase shapes, alternated with 64 reference measurements. The signal traces are based on total amounts of counts between 50 and 200 kcts per point. For the data in Fig. 4, the cycle consisted of 36 delay measurements, interleaved with 36 reference measurements. This cycle was repeated five times; the signal traces are based on a total amount of counts between 12 and 35 kcts per point. For the phase determination we use a least-squares fit in a basis of Lorentzian resonances where the number of resonances, their central wavelengths, their widths, and their relative weights are free parameters.

The signal error bars in all graphs are the magnitude of deviations of the 64 reference measurements to their average. The error bars for Fig. 3 also hold for Fig. 2 and are 1.5%; note that in Fig. 2, although the measurements were performed on individual antennas and the stated error holds for that, the graph shows the average signature of three antennas to enhance the signal to noise. The δ error bars in Fig. 3 reflect the calibration accuracy for the Fourier limited pulse: The residual phase after compression was flat to within 0.1π radian. This error practically falls away in the significantly larger phase added to the pulse in Fig. 4: -500-fs^2 chirp gives a quadratic phase function with a range of 5π radians throughout the pulse spectrum; the error resulting from the uncertainty in compression amounts to a 2% uncertainty in delay (i.e., maximum ±2 fs at 100-fs delay). The signal error bars in Fig. 4 are also determined by the deviation of the reference measurements to their average and are in the range of 6% owing to the shorter integration time and the division between two traces.

For the phase measurements on the nano-antennas, consider the following. For a pulse with complex spectrum centered at ω_0 and spectral amplitude and phase $E(\Delta)e^{i\varphi(\Delta)}$ at $\Delta = \omega - \omega_0$, the probability of a two-photon absorption (PTP) at a particular frequency $\omega_{TP} = 2(\omega_0 + \Delta)$ depends on the constructive addition of photons that have a combined energy ω_{TP}. PTP(Δ) then depends on the fundamental spectral amplitude and phase as follows (2):

$$PTP(\Delta) \propto \left| \int |E(\Delta+\Omega)||E(\Delta-\Omega)| e^{i[\varphi(\Delta+\Omega)+\varphi(\Delta-\Omega)]} d\Omega \right|^2, \quad \textbf{[S1]}$$

where the integration variable Ω is a detuning from the central frequency ω_0 similar to Δ.

Assuming continuous phases, $\varphi(\Delta+\Omega)+\varphi(\Delta-\Omega)$ can be expanded into a Taylor series where the second derivative of the phase is the first term that does not integrate out in Eq. **S1**. This tells us that the PTP at a particular frequency $\omega_{TP} = 2(\omega_0+\Delta)$ is determined by the second derivative of the spectral phase at frequency Δ. We add a shifting cosine function to the excitation pulse: $\varphi_{shaper}(\Delta) = \alpha \cos[\beta\Delta + \delta]$ (Fig. 1*B*). α is the amplitude of the phase function and determines the resolution with which the phase can be retrieved; $2\pi/\beta$ is the periodicity of the phase function in frequency space, determining the bandwidth over which the phase can be measured; δ is a phase offset. The cosine function has two well-defined points per period where

$\varphi''_{shaper}(\Delta) = 0$, namely in the zero crossings. These are scanned through the spectrum by varying the frequency offset δ (Fig. 1*B*). Appropriate tuning of β ensures that for a variation of δ from 0 to 2π, both zero crossings traverse the spectrum one after the other. To understand the measurement, it is important to compare two cases: without and with antenna dispersion.

Without dispersion, the zero crossings of the cosine in $\varphi_{shaper}(\Delta)$ determine the frequencies in the spectrum that dominate the PTP, because those frequencies are the only ones that are phase-matched. The TPPL signal we measure depends on the total probability of generating a two-photon excitation in gold. This is proportional to the spectrally integrated PTP and is in the zero-dispersion case therefore dominated by the phase-matched frequency, which is directly given by δ through $\phi''_{shaper}(\Delta) = 0 \rightarrow \omega - \omega_0 = \frac{\delta \pm \pi/2}{\beta}$. When dominated by the shaper phase, the TPPL response as a function of δ therefore traces the fundamental spectrum twice (Fig. S1).

With antenna dispersion, the relative contribution of the affected wavelengths to the PTP will change, which will be reflected in the TPPL response as a function of δ (Fig. 1 *C* and *D*). This trace therefore provides a signature of the antenna dispersion: For each δ, the integrated PTP will be dominated by the frequencies for which the total dispersion happens to be minimal. The shape of the signature will therefore deviate from the fundamental spectrum. Applying prior knowledge about the amplitude and phase of the fundamental spectrum (i.e., the residual phase is 0) therefore allows a fit to the signature and consequently retrieving the spectral phase.

For the pump-probe experiment the intensity of the TPPL signal in the hotspots is recorded as a function of the delay between the chirped pump pulse and a Fourier limited probe pulse, with both pulses having the same spectrum. This double pulse was created in the pulse shaper. To avoid fast interference fringes, the probe pulse was phase-locked to the central frequency of the band it was overlapping in the chirped pump pulse at each delay (Fig. 4*A*). The total probability for a two-photon excitation in each hotspot depends on the initial spectrum of the pulse (Fig. 1*A*), the chirp added in the pump pulse (-500 fs^2), the amplitude and phase profiles in the hotspots (Fig. 3), and the delay and phase between the pump and the probe pulse (Fig. 4*A*). The theoretical curve was calculated by integrating the PTP for each pump-probe pair in both hotspots, and dividing the two values.

For our purpose, noncrystalline gold antennas are attractive because they show very little direct second harmonic signal, which means that they will not pollute the coherent signals one tries to create, enhance, influence, or probe with the antenna. They do, however, provide a large TPPL signal. TPPL has been used as a characterization tool for hotspots from the earliest works on plasmonics (3). This is a great way to obtain nonlinear information about the ultrafast dynamics in hotspots without interfering with measurements one wishes to do with the antenna structures. The good qualitative agreement in the trend between the signatures measured on the single-antenna bars and calculated for the reconstructed resonances (Fig. 2 of the main text) demonstrates that viable phase information can be extracted from the TPPL measurements of the antenna signatures. However, the contrast in the measured signatures is markedly less than that in the calculated signatures. This can be for several reasons. First, liquid crystal-based phase shapers work under the approximation that a particular pixel in the liquid crystal (LC) corresponds to a particular wavelength in the spectrum. In reality, however, each pixel will receive a band of wavelengths determined by the pixel size and the N.A. of the optics focusing the light on the LC. Hence, each wavelength will be focused on a band of pixels determined by the same parameters. As a consequence of this, a phase function added in the shaper $\phi(\omega)$ transforms to the actual phase function $\varphi(\omega)$ given by $\varphi(\omega) = \int \phi(\Omega) g(\omega - \Omega) d\Omega$, where ideally $g(\omega) = \delta(\omega)$, the Dirac delta function, but in reality is a function with a finite width. Effectively this means that amplitude α of the applied function will become slightly lower than in theory, limiting the contrast in the recorded signature.

Another source of limited contrast is the phase noise in the excitation pulse. When the residual phase in the spectrum fluctuates, it is possible to obtain a PTP with the correct shape by integrating long enough, but the total power in the integrated PTP will be lower and the effective amplitude α of the added phase function will go down with the width of the noise band.

Finally, an interesting possibility was posited by Biagoni et al. (4) that an intermediate state in the gold is involved in the generation of TPPL. The exact dependency of a TPPL signal on this state is elusive; it shows varying behavior depending on pulse widths, peak powers, central wavelengths, and so on. The variation in the signatures clearly shows a phase dependence of the TPPL signal, but a short-lived intermediate level is a likely candidate in accounting for the loss in contrast in the measured signal compared with theory. However, a full treatment of its causes and influences goes beyond the scope of this paper.

1. Castro-Lopez M, Brinks D, Sapienza R, van Hulst NF (2011) Aluminum for nonlinear plasmonics: Resonance-driven polarized luminescence of Al, Ag, and Au nanoantennas. *Nano Lett* 11(11):4674–4678.
2. Lozovoy VV, Pastirk I, Dantus M (2004) Multiphoton intrapulse interference. IV. Ultrashort laser pulse spectral phase characterization and compensation. *Opt Lett* 29(7):775–777.
3. Beversluis M, Bouhelier A, Novotny L (2003) Continuum generation from single gold nanostructures through near-field mediated intraband transitions. *Phys Rev B* 68:115433.
4. Biagioni P, et al. (2009) Dependence of the two-photon photoluminescence yield of gold nanostructures on the laser pulse duration. *Phys Rev B* 80:45411.

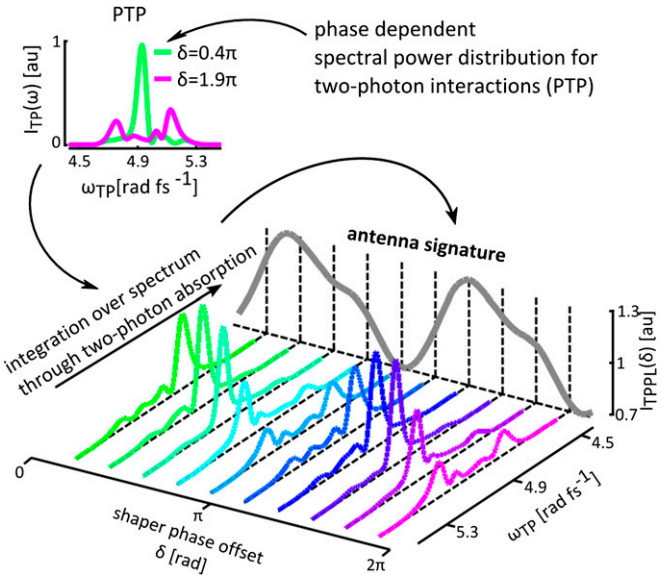

Fig. S1. Mapping the antenna phase in a TPPL signature. (*Inset*) The PTP for each δ is dominated by the frequency ω_{TP} for which the second derivative of the total spectral phase $\varphi''(\Delta) = 0 : I_{TP}$ is sharply maximum for this frequency. In the main figure, spectrally integrating the PTP for each δ, through two-photon absorption, traces this characteristic behavior into a phase signature. Without antenna dispersion, this signature tracks the shape of the fundamental spectrum twice (gray line). With antenna dispersion, integrating the PTP for each δ provides an antenna signature that differs from the zero dispersion case in a characteristic way and therefore provides a direct measurement of the spectral phase that the antenna adds to the field in the hotspot (see also Fig. 1 *C* and *D*).